ACS APPLIED MATERIALS & INTERFACES

Research Article

www.acsami.org

Photoassisted Enhancement of the Electrocatalytic Oxidation of Formic Acid on Platinized TiO_2 Nanotubes

Nazrul Mojumder,[†,§] Swagotom Sarker,[†,§] Syed Arslan Abbas,[†] Zong Tian,[‡] and Vaidyanathan (Ravi) Subramanian*[,†]

[†]Department of Chemical and Materials Engineering and [‡]Department of Civil and Environmental Engineering, University of Nevada, Reno, Nevada 89557, United States

Supporting Information

ABSTRACT: A solvothermal method is used to deposit Pt nanoparticles on anodized TiO_2 nanotubes (T_NT). Surface characterization using SEM, EDX, and XRD indicates the formation of polycrystalline TiO_2 nanotubes of 110 ± 10 nm diameter with Pt nanoparticle islands. The application of the T_NT/Pt photoanode has been examined toward simultaneous electrooxidation and photo(electro)oxidation of formic acid (HCOOH). Upon UV−vis photoillumination, the T_NT/Pt photoelectrode generates a current density of 72 mA/cm^2, which is significantly higher (~39-fold) than that of the T_NT electrode (1.85 mA/cm^2). This boosting in the overall current is attributable to the enhanced oxidation of formic acid at the T_NT/Pt-electrolyte interface. Further, a series of cyclic voltammetric (CV) responses, of which each anodic scan is switched to photoillumination at a certain applied bias (i.e., 0.2 V, 0.4 V, etc.), is used to identify the role of T_NT/Pt as a promoter for the photoelectrooxidation of formic acid and understand a carbon monoxide (CO)-free pathway. Chronoamperometric (j/t) measurements demonstrate the evidence of an external bias dependent variation in the time lag during the current stabilization. An analysis of the CV plots and j/t profiles suggests the existence of both the charge-transfer controlled process and the diffusion-controlled process during formic acid photoelectrooxidation.

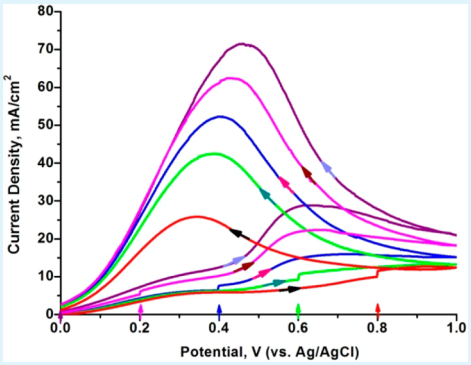

KEYWORDS: *TiO_2 nanotubes, solvothermal, Pt nanoparticles, formic acid, fuel cell, photoelectrocatalysis*

1. INTRODUCTION

A polymer electrolyte membrane fuel cell (PEMFC) is a device that can be used to convert high energy density fuels to electricity with high efficiencies compared to conventional internal combustion engines.[1−3] The basic electrochemical process in a PEMFC involves the following: an oxidative conversion of an energy source to a variety of products at the electrocatalyst-fuel interface and the subsequent abstraction of electron flow that constitutes current. It has been recently shown that the boosting of this electrocatalytic process is possible by combining the electrocatalyst with an underlying photocatalyst and photoillumination.[4] Most reports on this boosting approach discuss the application of alcohol as a fuel, precious group metal (PGM) as electrocatalyst, and 0D TiO_2 as the underlying photoactive material.[5−7] However, evidence of the application of this synergistic approach to the following critical areas is limited; thus, it underlies the need for a more systematic study. First, the viability of the approach to utilize the fuel of other classes such as the acid group has to be explored and understood clearly.[8−10] Second, since photocatalysis is involved, it is crucial to determine the applicability of 1D photoactive component as an alternative substrate. Moreover, the electrode−electrolyte interfacial processes that contribute toward enhancing the photooxidation of the fuel have to be clearly identified.

This study focuses on examining the usefulness of 1D TiO_2 nanotubes (T_NT) as the underlying substrate. T_NT is of relevance for its superiority as a photo(electro)catalyst compared to its particulate counterparts.[11,12] It is reported that the 1D T_NT offers higher active surface-to-volume ratio in comparison with TiO_2 nanoparticulate structure. Thus, it accommodates more oxidizing species at the T_NT-electrolyte interface.[13,14] Moreover, T_NT improves electron−hole pair separation and, thereby, transport of photogenerated electrons.[15] T_NT has been used as a substrate with metal nanoparticles.[16] Further, the multifunctionality of T_NT and its role in a composite toward solar energy conversion is well documented from our contributions[17−21] and by others.[22,23] On another note, weak acids are an upcoming category of benign energy source that can produce electricity using fuel cells. Among them, formic acid, a well-established portable energy source in fuel cells, is preferred since oxidation of single C-atom molecule is significantly less energy intensive.[24,25] Unlike methanol, formic acid has been less studied although it offers significant advantages in a fuel cell. A key reason in support of formic acid is the high fuel utilization efficiency due

Received: December 30, 2013
Accepted: March 18, 2014
Published: March 18, 2014

   dx.doi.org/10.1021/am406040v | ACS Appl. Mater. Interfaces 2014, 6, 5585−5594

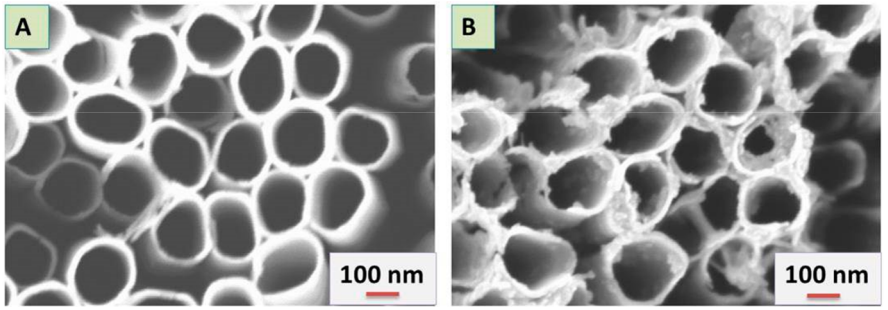

Figure 1. SEM images - (A) TiO_2 nanotubes (T_NT) and (B) T_NT with the solvothermal deposits synthesized at 140 °C over 4 h.

to minimal membrane crossover flux.[26] This results in a very low mixed potential at the cathode compared to methanol (attributable to the repulsion between the formate anion and the sulfonic group of the Nafion membrane).[27] However, formic acid has a lower energy density than methanol. Utilizing it in high concentrations can offset this issue.[28] Other advantages of formic acid as a fuel include amenability to oxidation using non-PGM metals, applicability of CO tolerant oxidation catalysts, and its availability from wide ranging sources.[29−31] Application of a wide bandgap semiconductor (a photocatalyst)[32,33]and noble metals (or their alloys) for formic acid oxidation has been extensively studied. It is reported that Pt decorated Au porous nanotubes show enhanced tolerance to CO poisoning.[34]In addition, various groups have demonstrated that composites of Pt and Au[35,36]show significant improved results toward formic acid oxidation. Beyond the use of Pt for formic acid oxidation, Pd/C[37]composite demonstrates catalytically active and stable performance. In recent times, graphene oxide support noble metal catalysts such as Pd/graphene oxide[38−40] and PtAu/graphene[41,42] are showing promising results.

In this work, we address the aforementioned aspects of formic acid utilization as a fuel and the effects of T_NT/Pt composite electrode in promoting oxidation. The parameters, that play critical roles in influencing formic acid oxidation at the T_NT/Pt interface, will also be identified. The synthesis of the composite using a solvothermal approach is discussed. The simultaneous electrooxidation and photoelectrooxidation of formic acid over the T_NT/Pt surface are systematically examined. The results obtained from implementing photoelectrochemical techniques offer mechanistic insights on the effects of photoillumination at various applied biases.

2. EXPERIMENTAL SECTION

2.1. Chemicals. Ethylene glycol (99.9%), ammonium fluoride (ACS Reagent ≥98%), chloroplatinic acid hexahydrate (ACS Reagent ≥37.50% Pt basis), sodium hydroxide (98%), deionized water, methanol (HPLC grade), formic acid (88%), and sulfuric acid (95−98% assay) were used.

2.2. Synthesis of TiO_2 Nanotubes. Titanium foil (99.7%, thickness of 0.13 mm) was used to prepare the TiO_2 nanotubes. The titanium substrate was polished; it was degreased with *iso*-propanol and, then, acetone in an ultrasonicator for some time. The electrolyte used for the anodization was a fluorinated solution (0.5% w/w) of ethylene glycol and DI water (10% w/w). Additional details of the synthesis can be found elsewhere.[43] Anodization was performed using a DC power source at an applied bias of 40 V for 2 h and platinum was used as the cathode. Anodized samples were annealed in air (furnace) at 450 °C for 2 h to obtain the desired crystallographic phase of TiO_2 nanotubes.

2.3. Formation of the T_NT/Pt Composite by a Solvothermal Method. Platinum was deposited on the T_NT surface by the reduction of the chloroplatinic acid hexahydrate in a pressure-based solvothermal reactor (Parr Instruments, 4748). The solution for the solvothermal method consisted of chloroplatinic acid hexahydrate (0.20 mM) and 1 mmol of NaOH dissolved in a mixture of 50 mL of methanol as a reducing agent and 10 mL of DI water. A 4.0 cm × 0.8 cm anodized titanium dioxide strip was placed vertically at the center of the reactor. The reactor was sealed and set in a furnace at 140 °C for 4 h. Later, it was cooled to room temperature by the natural air convection process, and the composite was obtained for further analysis.

2.4. Surface and Photoelectrochemical Measurements. A Scanning Electron Microscope (SEM), Hitachi S-4700, which is equipped with an OXFORD X-ray energy-dispersed spectrometer, was used to gather ultrahigh resolution (UHR) SEM images. Images were recorded with the help of a through-lens SE detector, which was located at a working distance of 4 mm and operated under an accelerating voltage of 3 kV. X-ray diffraction pattern was obtained using the Philips1204S B/3 diffractometer at a scan rate of 1°/min. Photoelectrochemical measurements were performed using an Autolab 30 Potentiostat/Galvanostat. Photoelectrochemical studies were carried out in a three-electrode cell − T_NT and T_NT/Pt as the working electrode, Pt wire as the counter electrode, and Ag/AgCl (in 3.4 M KCl) as the reference electrode. To study formic acid oxidation, formic acid (1.0 M) with H_2SO_4 (0.5 M) was used as the electrolyte. A 500 W Newport Xenon lamp worked as the light source. Cyclic voltammetric and chronoamperometric measurements were performed to understand the photoinduced catalytic property of the composite.

3. RESULTS

3.1. Surface Characterization of the Composite. *3.1.1. SEM Analysis.* Physical features of the composite were examined using a scanning electron microscope. The representative SEM images shown in Figure 1 were taken before (A) and after (B) the solvothermal process. The nanotubes are tubular, hollow, and aligned next to one another with a distinct intertubular spacing (Figure 1A). The diameter of the nanotubes is approximately 100 ± 10 nm, and the thickness of the nanotube wall is about 10 nm. The temperature and pressure assisted solvothermal process results in the formation of minute islands of the deposits on the nanotube surface. A change in the coloration of the sample before and after solvothermal treatment confirms the formation of deposits on the T_NT surface (see S 1). Deposited particles appear as discontinuous islands distributed along the surface of the T_NT (Figure 1B). The SEM image indicates that the solvothermal process-assisted deposition offers an alternative methodology (besides electrodeposition)[10,44] to form nanoparticles on the nanotubes.

3.1.2. XRD Analysis. The XRD spectrum of the synthesized composite is shown in Figure 2. The presence of the anatase

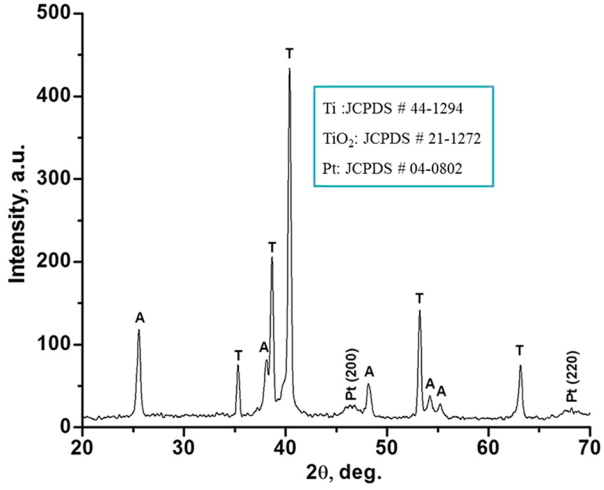

Figure 2. XRD pattern of the composite indicating the presence of titanium (T) and anatase TiO_2 (A). The presence of platinum was evident in the form of a short and broad peak indicated by Pt.

TiO_2 (designated as "A" in the spectrum) is evident. This is indexed to the JCPDS file # 21-1272. The presence of elemental titanium (designated as "T" and indexed to the JCPDS file # 44-1294) is also noted. The signals from the possible platinum deposit on the T_NT surface appear to be suppressed by the intense elemental titanium peak. The (111) plane of the deposited Pt, the strongest peak, is overlapped by the elemental titanium peak at $2\theta = 39.76°$. Other peaks of Pt within the XRD scan range can be identified (at $2\theta = 47°$ and 68°). They are attributed to the (200) and (220) planes, respectively. Therefore, the results for the Pt presence can be indexed to the JCPDS file # 04-0802. It is noteworthy that the broad width of these signals suggests the nanoscale range particle formation; it is consistent with the SEM analysis.

3.1.3. EDX Analysis. EDX analysis is performed to identify the elements that are present in the solvothermally synthesized composite. Figure 3 shows the EDX spectrum of the detected

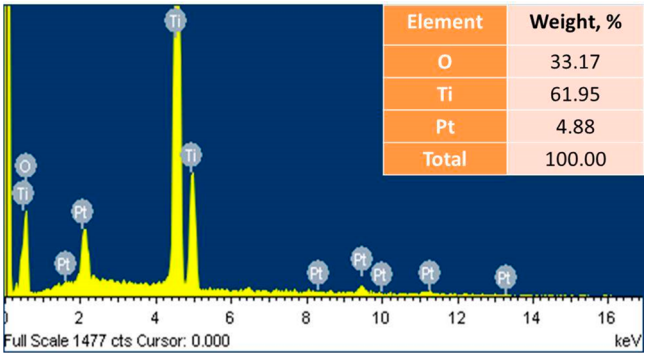

Figure 3. EDX spectroscopic results indicate the elements identified as Ti, Pt, and O. The analysis was carried out over a representative area of the composite.

elements over a representative area of the composite. The presence of platinum on the T_NT surface is confirmed from the results. Other elements, that are identified, are titanium and oxygen. The quantitative estimate of the Pt content for the representative EDX scan is ~4.88%. The composition of the other elements is shown in Figure 3 (inset). It is noteworthy to mention that the photocatalytic applications involving precious metal over an oxide surface typically demonstrate optimal results at a loading of <10 wt %.[45−47] In summary, physical appearance (black coloration − S 1),[48−52] XRD, and EDX analysis suggest the formation and deposition of platinum nanoparticles on the T_NT surface.

3.2. Electrochemical Characterization. *3.2.1. Carbon Monoxide (CO) Oxidation.* CO-oxidation[53] is a standard electrochemical technique for the estimation of active Pt sites.[54−56] One CO molecule adsorption at one Pt site is assumed during the electrochemical surface area estimation. The process provides the actual surface area of Pt available for formic acid electrooxidation. The experiment is performed using a 0.5 M sulfuric acid solution saturated with CO (CO was bubbled through the sulfuric acid solution for 25 min).[30,57,58] Figure 4 shows the cyclic voltammogram of the CO oxidation

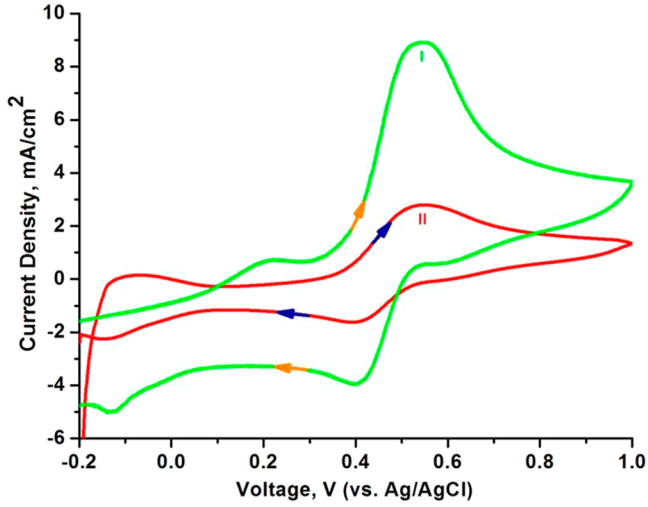

Figure 4. CO oxidation was performed to estimate the electrochemical surface area of Pt deposits on the T_NT [(I) first scan and (II) second scan]. A charge-to-area equivalent to 420 $\mu C/cm^2$ was used. The electrolyte was 0.5 M H_2SO_4. It was deaerated with N_2 and, later, saturated with CO for 25 min.

process over the T_NT/Pt composite. Although hydrogen desorption peaks seem to be suppressed in the first scan, both adsorption and desorption peaks of hydrogen are visible in the following scan shown in Figure 4.[59−61] The first scan with a peak at 0.55 V corresponds to the oxidation of the adsorbed CO as per the equation $Pt - CO_{ads} \xrightarrow{electrooxidation} Pt + CO_2$. The minor presence of the peak in the subsequent scan shows that the almost entire adsorbed CO is oxidized. The active area of the deposited Pt is determined using a charge-to-surface-area equivalent for CO oxidation on Pt as 420 $\mu C/cm^2$.[62,63] However, controlled experiment with plain TiO_2 nanotubes showed no CO-oxidation peak indicating that the CO oxidation on T_NT is below the detection limit.

3.3. Formic Acid Electrooxidation and Photoelectrooxidation. To decouple the photodriven process from the electrocatalytic process, formic acid oxidation measurements were performed separately under dark (electrochemical) and UV−vis photoillumination (photoelectrochemical) condition using T_NT and T_NT/Pt photoanodes. The results are discussed below.

3.3.1. Electrocatalysis and Photoelectrocatalysis of Formic Acid over T_NT. The electrochemical response of the bare T_NT photoanode toward formic acid oxidation in the absence

dx.doi.org/10.1021/am406040v | ACS Appl. Mater. Interfaces 2014, 6, 5585−5594

and the presence of photoillumination is shown in Figure 5. There is negligible current observed in the absence of

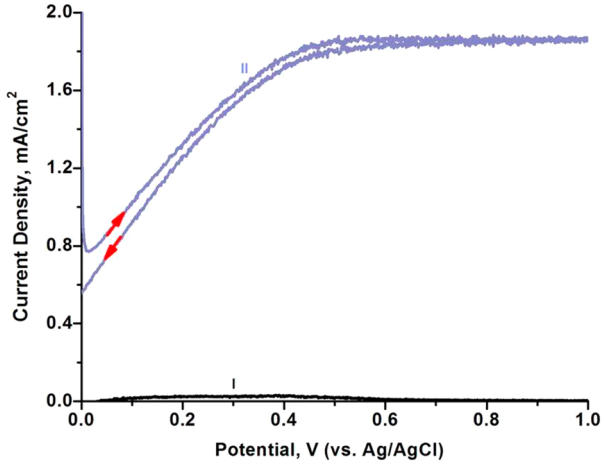

Figure 5. CV plots of the bare T_NT electrode in (I) the absence and (II) the presence of photoillumination. [Electrolyte: 1 M HCOOH + 0.5 M H_2SO_4; scan rate: 10 mV/s].

photoillumination, indicating that the electrocatalytic activity of the T_NT is mostly nonexistent. Formic acid is not known to demonstrate electrocatalytic activity over TiO_2.[64] Since there is no response here, this result is in line with expectations. However, upon UV−vis photoillumination, a saturation current density of 1.85 mA/cm^2 is noted. This indicates that the photoactivity is present but minimal.

In the photocatalytic process, the e^--h^+ pair is generated in the conduction (CB) and valence band (VB) of TiO_2 upon UV−vis photoillumination as shown in eq 1. The photocatalytic oxidation of formic acid is initiated by the holes formed in TiO_2. These holes directly or indirectly ($h^+ + OH^- \rightarrow OH^\bullet$) oxidize the formic acid (eq 2) to various byproducts.[47,65,66]

$$TiO_2 \xrightarrow{UV\ light} TiO_2\ (h^+_{VB} + e^-_{CB}) \quad (1)$$

$$HCOOH + TiO_2\ (h^+) \rightarrow oxidized\ product(s) + e^- \quad (2a)$$

$$HCOOH + OH^\bullet \rightarrow oxidized\ product(s) + e^- \quad (2b)$$

3.3.2. Electrocatalysis and Photoelectrocatalysis of Formic Acid over T_NT/Pt. The activity of the T_NT/Pt electrode toward formic acid oxidation was also examined in the absence of photoillumination as shown in Figure 6A. The measured current density shows a peak at about 0.32 V with a maximum current density of 10.65 mA/cm^2 (anodic scan), which is significantly higher than that of bare T_NT (1.85 mA/cm^2). The difference in the current density noted from Figure 5 (dark) and Figure 6A (dark) can be attributed to the nonphotocatalytic electrooxidation of formic acid over the solvothermally deposited platinum nanoparticles.

The electrocatalytic reaction on Pt follows two mechanisms: a 1-step direct pathway (dehydrogenation - eq 3) and 2-step indirect pathways (dehydration or formate pathways - eq 4) as shown below.[67−70]

Direct

$$HCOOH \xrightarrow{Pt} 2H^+ + CO_2 + 2e^- \quad (3)$$

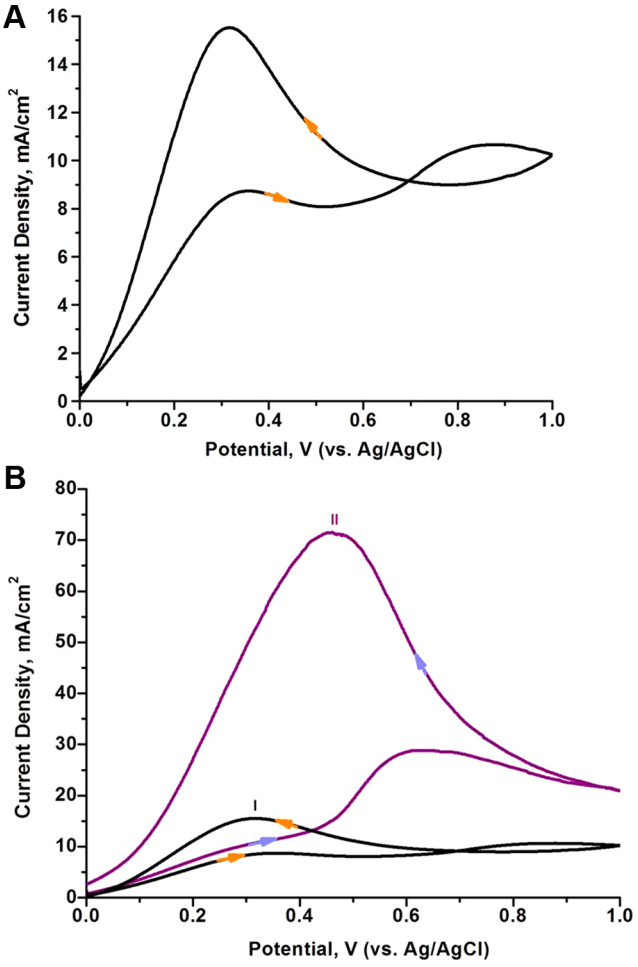

Figure 6. A. CV plot of the T_NT/Pt electrode in the absence of photoillumination. [Electrolyte: 1 M HCOOH + 0.5 M H_2SO_4; scan rate: 10 mV/s]. B. CV plots of the T_NT/Pt electrode in (I) the absence and (II) the presence of photoillumination. [Electrolyte: 1 M HCOOH + 0.5 M H_2SO_4; scan rate: 10 mV/s].

Indirect (CO path)

$$HCOOH \rightarrow H_2O + CO \quad (4a)$$

$$CO \xrightarrow{Pt-OH} H^+ + CO_2 + e^- \quad (4b)$$

Indirect ($HCOO_{ads}$ path)

$$HCOOH \xrightarrow{-H^+,-e^-} HCOO_{ads} \quad (4c)$$

$$HCOO_{ads} \xrightarrow{-H^+,-e^-} CO_2 \quad (4d)$$

The forward scan (Figure 6A) shows its first peak ~0.35 V, which is attributable to formic acid oxidation via a combination of processes given in eqs 3 and 4.[71−73] The plateau in the current above 0.35 V is indicative of loss of the Pt activity via CO poisoning as per eq 4a. At further positive potential, an increase in the current is again observed. This is attributable to oxidation of the adsorbed CO on Pt sites.[74,75] The subsequent plateau in this current is for Pt oxidation.[62,72] The scan was terminated at 1.0 V to avoid extensive Pt oxidation and oxygen evolution (noted commonly at further positive potential). In the reverse scan, the oxidized Pt is partially reduced and becomes available for further electrocatalytic oxidation of

formic acid or other intermediate species (eq 4).[71−73] The higher current density peak with a magnitude of ∼16 mA/cm^2 at 0.3 V during the reverse scan is attributable to further oxidation of formic acid and/or additional intermediates/surface oxides.[76,77]

Of greater importance is the result noted upon UV−vis photoillumination of T_NT/Pt photoanode as shown in Figure 6B. Formic acid electrooxidation is evident from the characteristic peak observed in the voltammogram. In the forward scan of T_NT/Pt, the anodic peak is noted at 0.60 V. In the reverse scan, the characteristic peak is noted at 0.42 V. The current density significantly increases to 72 mA/cm^2 in the presence of photoillumination; thus, it shows a 4.5-fold increase in comparison with the result (reverse scan) of Figure 6A. The boosting in the photocurrent density may be attributed to the combined contributions from the reactions mentioned in eqs 1-4). These contributions are further examined in detail in section 4.

3.3.3. Chronoamperometry (j/t) of the T_NT/Pt Electrode. Since the anodic and cathodic scans showed a potential dependent variation in the photocurrent, a chronoamperometric analysis was performed at various potentials using the T_NT/Pt electrode and the same electrolyte in the absence and the presence of photoillumination. This analysis provides time-resolved (photo)electrocatalytic response of the T_NT/Pt and offers insight into the stability of the generated current. Representative chronoamperometric measurements performed at different applied potentials (0.30, 0.45, and 0.70 V) are shown in Figure 7. The dashed lines in the figure indicate the current density obtained due to formic acid electrooxidation in the absence of photoillumination. Pt contributes to the oxidation process resulting in a relatively stable current over the scan period.

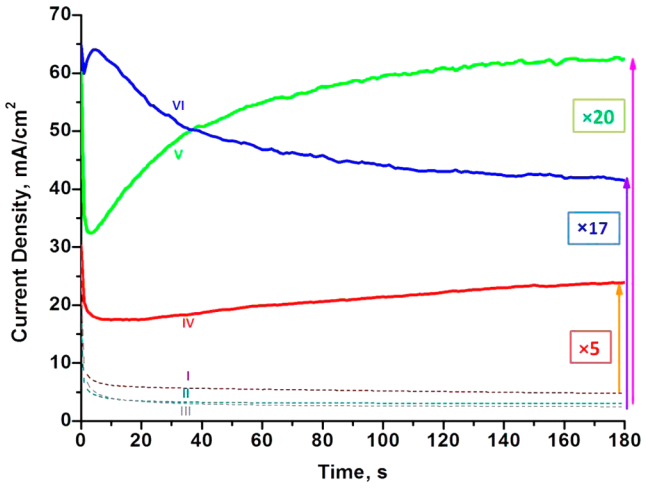

Figure 7. Chronoamperometric plots of the T_NT/Pt electrode under an applied bias of (I, IV) 0.30 V, (II, V) 0.45 V, and (III, VI) 0.60 V. Dark current and photocurrent densities are shown respectively by the dotted and continuous lines. [Electrolyte: 1 M HCOOH + 0.50 M H_2SO_4].

Upon photoillumination, at an applied bias of 0.30 V, the current density increases to 23.9 mA/cm^2, which is a 5-fold higher value than the response obtained under dark conditions. For an applied bias of 0.45 V, the current density increases up to 62.5 mA/cm^2; whereas, at the end of the same scanning period, the j/t response yields only 3.04 mA/cm^2 in the absence of illumination. A relatively stabilized value of the photocurrent density is noticed at an applied bias of V = 0.70 V after the scanning period of 180 s; it is found to be 42.0 mA/cm^2. In comparison with the dark condition at the same bias, a 17-fold enhancement is observed. Chronoamperometric results for the formic acid (photo)electrooxidation with the T_NT/Pt electrode are detailed in Table 1. It includes current densities obtained in the absence and the presence of photoillumination after a scanning period of 180 s. The results of Figure 7 and Table 1 indicate a potential dependent enhancement in the current density, where magnitudes vary between 5- and 21-fold upon photoillumination. The significance of this observation is that if a photofuel cell were to be assembled and operated, any discharge potential of the cell could leverage the photoassisted boosting phenomenon and contribute to the enhancement of the overall device performance.

Table 1. Magnitude of Current Densities at Different Applied Biases for the T_NT/Pt Electrode in the Absence and the Presence of Photoillumination after a Stabilization Period of 180 s[a]

applied bias, V (V)	current density in the absence of light, j (mA/cm^2)	current density in the presence of light, j (mA/cm^2)	increase in current density, (fold)	"well-like profile", t (s)
0.30	4.79	23.9	5	180
0.45	3.04	62.5	20	130
0.50	2.88	61.6	21	90
0.60	2.59	49.8	19	15
0.70	2.49	42.0	17	5
0.80	2.43	38.4	16	3

[a]It also shows the time required for the current to stabilize in the "well-like profile" region.

4. DISCUSSIONS

4.1. Deciphering the Basis of Increase in the Current Density through Controlled Photoillumination. The forward and reverse scans of T_NT and T_NT/Pt photoanodes reported in Figures 5 and 6 are obtained either completely under dark or continuous photoillumination. It is evident that the higher current density is indicative of the synergistic coupling between photocatalytic and electrocatalytic processes; the contributions from these individual processes need to be decoupled and analyzed. Therefore, part of the scan range was performed under dark, and the remainder was exposed to continuous photoillumination. For clarity, only the anodic scans using the T_NT/Pt photoanode are shown in Figure 8A. The photoilluminated part of the scan range is varied as a function of voltage and arrows with the word "On" "are shown" to indicate the point, where the T_NT/Pt photoanode was exposed to UV−vis photoillumination.

In the absence of photoillumination, the current density observed in the anodic scans (Figure 8A) is attributed exclusively to the electrons generated due to the formic acid electrooxidation on Pt (eqs 3-4). However, as soon as the photoillumination is initiated at different potentials for the remainder of the scans, a short spike followed by an increase in the current density is observed. There are two interesting observations inferred from these anodic scans. First, the flat segment of the anodic scan disappears as the photoanode is subjected to the photoillumination at an earlier bias. Second, the longer the T_NT/Pt electrode is exposed to photo-

dx.doi.org/10.1021/am406040v | ACS Appl. Mater. Interfaces 2014, 6, 5585−5594

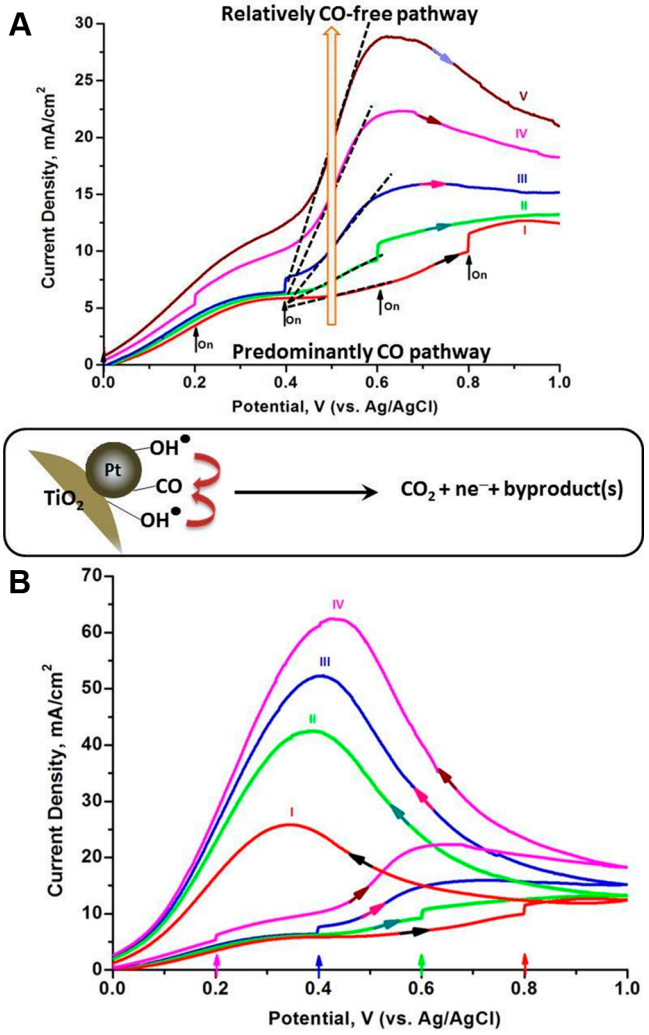

Figure 8. A. A series of forward scans of the T_NT/Pt electrode - each scan is subjected to the photoillumination at different biases: (I) 0.8 V, (II) 0.6 V, (III) 0.4 V, (IV) 0.2 V, and (V) 0 V. [Electrolyte: 1 M HCOOH + 0.5 M H_2SO_4; scan rate: 10 mV/s]. The schematic at the bottom of the figure indicates the mechanism of CO oxidation on the T_NT/Pt. B. CV plots of the T_NT/Pt electrode - each anodic scan is subjected to the photoillumination at different biases: (I) 0.8 V, (II) 0.6 V, (III) 0.4 V, and (IV) 0.2 V. The arrow in the plot indicates the point where the switch from the dark to the photoillumination is carried out. [Electrolyte: 1 M HCOOH + 0.5 M H_2SO_4; scan rate: 10 mV/s].

illumination, the greater is the number of electrons generated contributing to the increasing current density.

From the analysis of Figure 6A (section 3.3.2), the flat segment of the T_NT/Pt scan under dark (from 0.4 to 0.6 V) is indicative of CO poisoning of the Pt sites. The scans of Figure 8A indicate that these flat segments are replaced by a region with increasing slope (the dotted lines between 0.4 and 0.6 V) when photoillumination is started at an earlier bias. This increased slope in response to photoillumination is suggestive of not only the active Pt availability to enhance oxidation but also the progressive reduction of CO poisoning. Thus, under a longer period of photoillumination, the reduced CO poisoning effect can aide in prolonging the availability of active Pt sites (possible contribution to further oxidative processes). It is the basis for the increased current density.

4.2. Role of TiO_2 and Pt toward Promoting a CO-Free Pathway on Pt Surface. It is well reported that the water molecules are adsorbed on TiO_2 either in dissociated or undissociated forms[78−80] and Pt has the proven ability to generate hydroxyl species upon photoillumination from the water molecule.[81,82] Pt itself, in acid media, is known to promote water or OH driven oxidation of CO leading to the formation of various byproducts.[83,84] It is noteworthy that the Pt nanoparticles are present as discontinuous islands on T_NT surface (evident from Figure 1) and both of these are required to interact with adsorbed CO. Under this circumstance, it is clear that, if CO were to be bonded on the active Pt sites, it would be readily oxidized.[45] There are multiple CO-oxidation pathways (scheme of Figure 8A). They can ensure that CO buildup does not reach a point where a significant number of Pt sites is poisoned. Thus, the availability of active Pt sites for continued formic acid oxidation is ensured due to the T_NT presence, leading to higher current.

The reduced levels of CO poisoning confirm the availability of the active Pt sites. At the same time, the increased current generation suggests that the pathway for formic acid oxidation switches from a predominantly CO-based pathway (dehydration) to a relatively-CO-free pathway as indicated by the arrow. In fact, the benefits of such switching are more obvious in the reverse scan (shown in Figure 8B) than the corresponding forward scan. The current density in the reverse scans is attributed to the oxidation of formic acid and/or other intermediates (surface oxides) adsorbed/formed on Pt.[71,72] If the T_NT/Pt is subjected to the photoillumination at an earlier bias of the forward scan, an increased current density in the reverse scan is evident. This higher current density is attributable to the oxidation of surface oxides, formic acid, and/or associated intermediates (as per mechanism in eqs 3, 4c, or 4d). Thus, the presence of T_NT with its extended surface area and the controlled photoillumination during the anodic scan offers two benefits: prolonging Pt activity with minimal CO poisoning and contributing to a significant enhancement of the current generation.

4.3. Limited Contribution of TiO_2 and Pt through Traditional Roles. Photoinduced production of electron, especially under an external bias, is a well-reported phenomenon for TiO_2. Therefore, the performance of the T_NT electrode in the absence and the presence of photoillumination was also examined. When the TiO_2 electrode is subjected to the photoillumination, an enhancement in the current density is observed. The trend in increase in the current generation is similar to that of the T_NT/Pt electrode. However, the key observation is that the magnitudes of these current densities are similar to the results obtained for the T_NT/Pt electrode (S 2). This suggests that the number of photogenerated electrons contributing to the current is small.

Similarly, the role of Pt as a sink for photogenerated electrons in TiO_2 and thus promoting charge separation and transport is also well documented.[85] It forms a Schottky-type contact with TiO_2 that allows for efficient electron transfer across the TiO_2/Pt.[86] Thus, the increase in current upon photoillumination for the T_NT/Pt electrode could be well attributable to this role of Pt. However, if the observed spikes upon photoillumination for T_NT and T_NT/Pt were closely examined (Figure 8B and S 2), and compared (Table 2), the magnitude of the current density for the T_NT/Pt electrode appears to be similar to that of the T_NT electrode. It suggests that the role of Pt, even if present, is too small to make any

Table 2. Magnitude of Current Densities during Switching from the Dark Condition to the Photoillumination at Different Applied Biases for T_NT and T_NT/Pt Electrodes

applied bias, V (V)	current density forT_NT/Pt, j (mA/cm^2)	Δj for T_NT/Pt, (mA/cm^2)	current density for T_NT, j (mA/cm^2)	Δj for T_NT, (mA/cm^2)
0.2	5.30−6.11	0.81	0.04−1.10	1.06
0.4	6.43−7.45	1.02	0.03−1.65	1.62
0.6	9.22−10.3	1.08	0.02−1.63	1.61
0.8	9.95−11.5	1.55	0.00−1.68	1.68

significant contribution to the current in the external circuit according to the aforementioned manner.

4.4. Decoupling the Contributions from Electrocatalysis and Photoelectrocatalysis. The analysis presented in section 4.1 identifies electrocatalytic and photoelectrocatalytic processes to be the basis for the current generation. It also provides a general trend in the current generation as follows: $j_{T\_NT\ (UV)} < J_{T\_NT/Pt\ (Dark)} < J_{T\_NT/Pt\ (Photoillumination)}$. The magnitudes of the current density differ in the absence and the presence of photoillumination. The following question arises: *What is the relative contribution range from all of these processes.* Figure 9 shows a plot of the peak current densities for

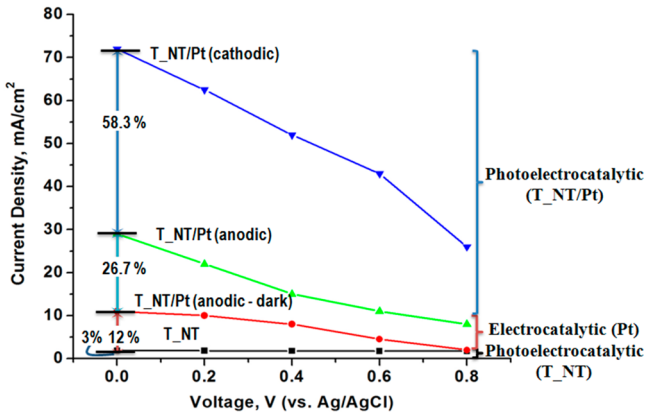

Figure 9. Identification of the contribution to current densities in the external circuit from the photoelectrocatalytic (T_NT), electrocatalytic (Pt), and photoelectrocatalytic (T_NT/Pt) processes.

T_NT and T_NT/Pt electrodes under dark and controlled photoillumination at various biases. Since the forward and reverse scans for T_NT/Pt result in varying currents, the peak current densities in both cases are shown. This plot summarizes the relative contribution of the current under different scenarios. From S 2 and the short spikes of Figure 8A the T_NT contribution is clearly notable, but it is still insignificant at any potential. However, its role in promoting the function of Pt in the presence of photoillumination is clearly evident. Also evident is the enhancement in the current using T_NT/Pt during the forward and reverse scans in the absence and the presence of photoillumination. Based on these observations, three zones of current contributions can be identified as shown in the figure: a very small photoelectrocatalytic zone with ∼3% activity attributable to the bare T_NT, an electrocatalytic zone with 9−12% attributable to Pt, and the combined effect of the composite electrode in response to photoillumination highlighted as the photoelectrocatalytic zone (T_NT/Pt).

4.5. Insights into the Current Stabilization Process at the T_NT/Pt-Electrolyte Interface. This section examines the reasons for different photocurrent profiles of the T_NT/Pt electrode under different applied biases during the scanning period of 180 s. S 3 shows a magnified section (first 20 s) of the chronoamperometric results. The prominent features in the profiles are (i) an immediate decrease in the current density followed by an increase (this feature is referred to a "well-like profile") and (ii) a narrow width of the well-like profile with the increase in the applied bias. Table 1 shows the span (time) for such well-like profile. First, the well-like profile seen in the chronoamperometry is examined. The application of a positive bias creates an external driving force for the photogenerated electrons to traverse across the anode to the cathode through the external circuit. This driving force typically increases with an increase in the applied bias resulting in a greater number of electron−hole pair separations. The net result is the higher current density as seen from the results. The decreasing time width of the well-like profile with the higher applied bias noted in Table 1 indicates that the driving force generated by the external bias reduces the current decay expeditiously. Further, higher current density with increased bias and the increased contribution of photoelectrocatalysis (Figure 9) warrant that higher formic acid oxidation occurs on the T_NT/Pt surface. The decrease in the current density after the well-like profile (Figure 7 and S 2) at higher biases puts a spotlight on the formic acid availability for photoelectrooxidation. The availability of the formic acid is dictated by the diffusion layer of the electrolyte. The increase in current density noted at 0.45 V compared to the 0.3 V after the well-like profile can be attributed to the anode half-cell operating with no mass transport limitation. However, the decrease in current observed at 0.70 V after the first 5 s suggests that the formic acid diffusion is not able to keep up with the demands of the photoelectrocatalysis. Thus, the trend in the chronoamperometry indicates a gradual shift from a charge-transfer controlled process to a diffusion-controlled (mass transport limitation) process as the applied bias is increased.[87] This phenomenon is illustrated in Scheme 1. One approach to limit the diffusion-controlled process could be to increase the concentration of the formic acid. Further work in this area may involve i) examining strategies to improve the solvothermal approach or ii) deposition of other catalysts that are reported to have superior electrocatalytic activity than Pt.

5. CONCLUSION

TiO_2 nanotubes with discontinuous islands of platinum nanoparticles were synthesized using a solvothermal approach and used as a photoanode to perform the electrooxidation of formic acid. Both electrocatalytic and photoelectrocatalytic processes are evident at the T_NT/Pt − electrolyte interface. A 5- to 21-fold external bias-dependent increase in the current density clearly represents the efficient utilization of the T_NT/Pt composite in the presence of UV−vis photoillumination via a combination of the two processes. Several insights from the photoelectrochemical performances of the T_NT/Pt electrode are gathered. First, a key highlight of formic acid electrooxidation with the T_NT/Pt electrode in response to the photoillumination is the identification of the relatively CO-free pathway. Second, three zones with their range of impact toward formic acid oxidation have been identified as follows: photoelectrocatalytic (bare T_NT), electrocatalytic (Pt), and photoelectrocatalytic (T_NT/Pt) zone. Third, an external bias dependent well-like profile in the chronoamperometry is evident, and the chronoamperometric current profiles are

dx.doi.org/10.1021/am406040v | ACS Appl. Mater. Interfaces 2014, 6, 5585−5594

Scheme 1. Characteristic "Well-like Profile" in the Chronoamperometry and the Subsequent Trend in the Current Densities[a]

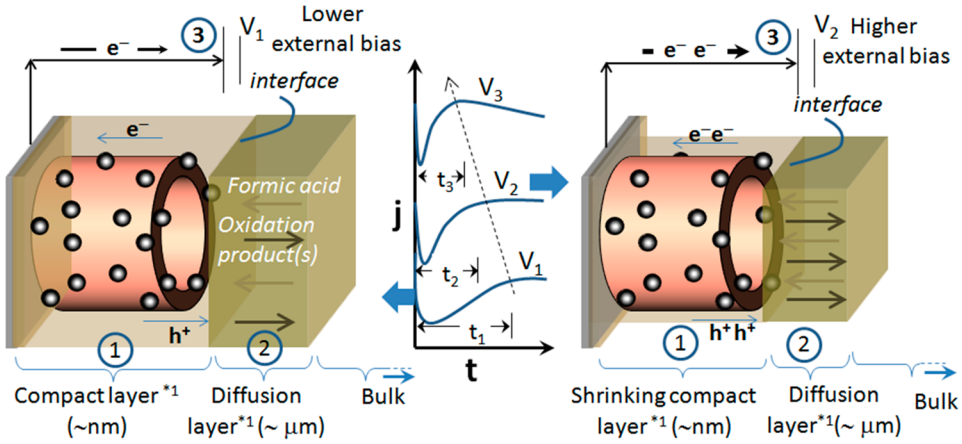

[a]At lower biases, the current density is predominantly a charge-transfer controlled process (region 1). At higher biases, it is observed to be dominated by the diffusion-controlled process (region 2). The combination of these two processes influences the total current in the external circuit (region 3). t_1-t_3 indicates the duration [Table 1 and S 3] of the "well-like profile". (*1. Thickness is not drawn up to the scale).

attributed to a combination of the charge-transfer controlled process and the diffusion-controlled process.

■ ASSOCIATED CONTENT

Supporting Information

Photographs of the samples, CV plots of T_NT electrode (where each anodic scan is subject to the photoillumination at different biases), and chronoamperometric results of the T_NT/Pt photoelectrode under various constant biases for 20 s. This material is available free of charge via the Internet at http://pubs.acs.org.

■ AUTHOR INFORMATION

Corresponding Author

*Phone: (775)-784-4686. Fax: (775)-327-5059. E-mail: ravisv@unr.edu.

Author Contributions

[§]These authors contributed equally to this research and manuscript preparation.

Notes

The authors declare no competing financial interest.

■ ACKNOWLEDGMENTS

R.S.V. acknowledges the technical discussions with Dr. Satyajit Gupta and Dr. Josephine Selvaraj. The financial support for N.M. provided by the Civil and Environmental Engineering Department, UNR through Dr. Z.T. and NSF-CBET-1337050 are acknowledged. R.S.V. also acknowledges the support for S.A.A. through the General Undergraduate Research Award (GURA) fellowship.

■ REFERENCES

(1) Arico, A. S.; Srinivasan, S.; Antonucci, V. DMFCs: From Fundamental Aspects to Technology Development. *Fuel Cells* **2001**, *1*, 133−161.

(2) Song, S. Q.; Maragou, V.; Tsiakaras, P. How Far Are Direct Alcohol Fuel Cells from Our Energy Future? *J. Fuel Cell Sci. Technol.* **2007**, *4*, 203−209.

(3) Yu, X. W.; Pickup, P. G. Recent Advances in Direct Formic Acid Fuel Cells (DFAFC). *J. Power Sources* **2008**, *182*, 124−132.

(4) Drew, K.; Girishkumar, G.; Vinodgopal, K.; Kamat, P. V. Boosting Fuel Cell Performance with a Semiconductor Photocatalyst: TiO_2/Pt-Ru Hybrid Catalyst for Methanol Oxidation. *J. Phys. Chem. B* **2005**, *109*, 11851−11857.

(5) Mor, G. K.; Carvalho, M. A.; Varghese, O. K.; Pishko, M. V.; Grimes, C. A. A Room-Temperature TiO_2-Nanotube Hydrogen Sensor able to Self-Clean Photoactively from Environmental Contamination. *J. Mater. Res.* **2004**, *19*, 628−634.

(6) Roy, P.; Berger, S.; Schmuki, P. TiO_2 Nanotubes: Synthesis and Applications. *Angew. Chem., Int. Ed.* **2011**, *50*, 2904−2939.

(7) Xin, Y. J.; Liu, H. L.; Han, L.; Zhou, Y. B. Comparative Study of Photocatalytic and Photoelectrocatalytic Properties of Alachlor Using Different Morphology TiO_2/Ti Photoelectrodes. *J. Hazard. Mater.* **2011**, *192*, 1812−1818.

(8) Hoffmann, M. R.; Martin, S. T.; Choi, W. Y.; Bahnemann, D. W. Environmental Applications of Semiconductor Photocatalysis. *Chem. Rev.* **1995**, *95*, 69−96.

(9) Bak, T.; Nowotny, J.; Rekas, M.; Sorrell, C. C. Photo-Electrochemical Hydrogen Generation from Water Using Solar Energy. Materials-Related Aspects. *Int. J. Hydrogen Energy* **2002**, *27*, 991−1022.

(10) Selvaraju, T.; Ramaraj, R. Electrochemically Deposited Nano-structured Platinum on Nafion Coated Electrode for Sensor Applications. *J. Electroanal. Chem.* **2005**, *585*, 290−300.

(11) Lin, C. J.; Yu, Y. H.; Liou, Y. H. Free-Standing TiO_2 Nanotube Array Films Sensitized with CdS as Highly Active Solar Light-Driven Photocatalysts. *Appl. Catal., B* **2009**, *93*, 119−125.

(12) Zhuang, H. F.; Lin, C. J.; Lai, Y. K.; Sun, L.; Li, J. Some Critical Structure Factors of Titanium Oxide Manotube Array in its Photocatalytic Activity. *Environ. Sci. Technol.* **2007**, *41*, 4735−4740.

(13) Shankar, K.; Basham, J. I.; Allam, N. K.; Varghese, O. K.; Mor, G. K.; Feng, X. J.; Paulose, M.; Seabold, J. A.; Choi, K. S.; Grimes, C. A. Recent Advances in the Use of TiO_2 Nanotube and Nanowire Arrays for Oxidative Photoelectrochemistry. *J. Phys. Chem. C* **2009**, *113*, 6327−6359.

(14) Yu, B. Y.; Tsai, A.; Tsai, S. P.; Wong, K. T.; Yang, Y.; Chu, C. W.; Shyue, J. J. Efficient Inverted Solar Cells Using TiO_2 Nanotube Arrays. *Nanotechnology* **2008**, *19*, 255202.

(15) Baker, D. R.; Kamat, P. V. Photosensitization of TiO_2 Nanostructures with CdS Quantum Dots: Particulate versus Tubular Support Architectures. *Adv. Funct. Mater.* **2009**, *19*, 805−811.

(16) Rettew, R. E.; Allam, N. K.; Alamgir, F. M. Interface Architecture Determined Electrocatalytic Activity of Pt on Vertically Oriented TiO_2 Nanotubes. *ACS Appl. Mater. Interfaces* **2011**, *3*, 147−151.

(17) Chen, W. Y.; Seiner, J.; Suzuki, T.; Lackner, M. *Handbook of Climate Change Mitigation*; Springer: New York, 2013; pp 1217−1262.

(18) Subramanian, V.; Sarker, S.; Yu, B.; Kar, A.; Xiaodi, S.; Dey, S. TiO_2 Nanotubes and Its Composites: Photocatalytic and Other Photo-Driven Applications. *J. Mater. Res.* **2013**, *28*, 279−292.
(19) Mukherjee, B.; Wilson, W.; Subramanian, V. TiO_2 Nanotube (T_NT) Surface Treatment Revisited: Implications of ZnO, $TiCl_4$, and H_2O_2 Treatment on the Photoelectrochemical Properties of T_NT and T_NT-CdSe. *Nanoscale* **2013**, *5*, 269−274.
(20) Smith, Y. R.; Subramanian, V. Heterostructural Composites of TiO_2 Mesh-TiO_2 Nanoparticles Photosensitized with CdS: A New Flexible Photoanode for Solar Cells. *J. Phys. Chem. C* **2011**, *115*, 8376−8385.
(21) Smith, Y. R.; Subramanian, V.; Viswanathan, B. *Photoelectrochemical and Photocatalytic Conversion of Carbon Dioxide*; Bentham Science Publishers: Osaka, 2010; pp 217−242.
(22) Yun, J. H.; Ng, Y. H.; Ye, C.; Mozer, A. J.; Wallace, G. G.; Amal, R. Sodium Fluoride-Assisted Modulation of Anodized TiO_2 Nanotube for Dye-Sensitized Solar Cells Application. *ACS Appl. Mater. Interfaces* **2011**, *3*, 1585−1593.
(23) Xie, Y.; Ali, G.; Yoo, S. H.; Cho, S. O. Sonication-Assisted Synthesis of CdS Quantum-Dot-Sensitized TiO_2 Nanotube Arrays with Enhanced Photoelectrochemical and Photocatalytic Activity. *ACS Appl. Mater. Interfaces* **2010**, *2*, 2910−2914.
(24) Lin, W. F.; Christensen, P. A.; Hamnett, A. The Electro-Oxidations of Methanol and Formic Acid at the Ru(0001) Electrode as a Function of Temperature: In-Situ FTIR Studies. *Phys. Chem. Chem. Phys.* **2001**, *3*, 3312−3319.
(25) Jusys, Z.; Behm, R. J. Methanol Oxidation on a Carbon-Supported Pt Fuel Cell Catalyst - A Kinetic and Mechanistic Study by Differential Electrochemical Mass Spectrometry. *J. Phys. Chem. B* **2001**, *105*, 10874−10883.
(26) Jeong, K. J.; Miesse, C. A.; Choi, J. H.; Lee, J.; Han, J.; Yoon, S. P.; Nam, S. W.; Lim, T. H.; Lee, T. G. Fuel Crossover in Direct Formic Acid Fuel Cells. *J. Power Sources* **2007**, *168*, 119−125.
(27) Rhee, Y. W.; Ha, S. Y.; Masel, R. I. Crossover of Formic Acid through Nafion (R) Membranes. *J. Power Sources* **2003**, *117*, 35−38.
(28) Ha, S.; Larsen, R.; Zhu, Y.; Masel, R. I. Direct formic Acid Fuel Cells with 600 mA cm^{-2} at 0.4 V and 22-C. *Fuel Cells* **2004**, *4*, 337−343.
(29) Larsen, R.; Masel, R. I. Kinetic Study of CO Tolerance during Electro-Oxidation of Formic Acid on Spontaneously Deposited Pt/Pd and Pt/Ru Nanoparticles. *Electrochem. Solid- State Lett.* **2004**, *7*, 148−150.
(30) Waszczuk, P.; Barnard, T. M.; Rice, C.; Masel, R. I.; Wieckowski, A. A Nanoparticle Catalyst with Superior Activity for Electrooxidation of Formic Acid. *Electrochem. Commun.* **2002**, *4*, 732−732.
(31) Neto, A. O.; Giz, M. J.; Perez, J.; Ticianelli, E. A.; Gonzalez, E. R. The Electro-Oxidation of Ethanol on Pt-Ru and Pt-Mo Particles Supported on High-Surface-Area Carbon. *J. Electrochem. Soc.* **2002**, *149*, 272−279.
(32) McMurraya, T. A.; Byrne, J. A.; Dunlop, P. S. M.; Winkelman, J. G. M.; Eggins, B. R.; McAdams, E. T. Intrinsic Kinetics of Photocatalytic Oxidation of Formic and Oxalic Acid on Immobilised TiO_2 Films. *Appl. Catal., A* **2004**, *262*, 105−110.
(33) Gazsi, A.; Schubert, G.; Pusztai, P.; Solymosi, F. Photocatalytic Decomposition of Formic Acid and Methyl Formate on TiO_2 Doped with N and Promoted with Au. Production of H_2. *Int. J. Hydrogen Energy* **2013**, *38*, 7756−7766.
(34) Gu, X.; Cong, X.; Ding, Y. Platinum-Decorated Au Porous Nanotubes as Highly Efficient Catalysts for Formic Acid Electro-Oxidation. *ChemPhysChem* **2010**, *11*, 841−846.
(35) Liu, J.; Cao, L.; Huang, W.; Li, Z. Preparation of AuPt Alloy Foam Films and Their Superior Electrocatalytic Activity for the Oxidation of Formic Acid. *ACS Appl. Mater. Interfaces* **2011**, *3*, 3552−3558.
(36) Wang, R.; Liu, J.; Liu, P.; Bi, X.; Yan, X.; Wang, W.; Ge, X.; Chen, M.; Ding, Y. Dispersing Pt Atoms onto Nanoporous Gold for High Performance Direct Formic Acid Fuel Cells. *Chem. Sci.* **2014**, *5*, 403−409.
(37) Mazumder, V.; Sun, S. Oleylamine-Mediated Synthesis of Pd Nanoparticles for Catalytic Formic Acid Oxidation. *J. Am. Chem. Soc.* **2009**, *131*, 4588−4589.
(38) Chen, X.; Wu, G.; Chen, J.; Chen, X.; Xie, Z.; Wang, X. Synthesis of "Clean" and Well-Dispersive Pd Nanoparticles with Excellent Electrocatalytic Property on Graphene Oxide. *J. Am. Chem. Soc.* **2011**, *133*, 3693−3695.
(39) Huang, H.; Wang, X. Pd Nanoparticles Supported on Low-Defect Graphene Sheets: For Use as High-Performance Electrocatalysts for Formic Acid and Methanol Oxidation. *J. Mater. Chem.* **2012**, *22*, 22533−22541.
(40) Jin, T.; Guo, S.; Zuo, J. J.; Sun, S. Synthesis and Assembly of Pd Nanoparticles on Graphene for Enhanced Electrooxidation of Formic Acid. *Nanoscale* **2013**, *5*, 160−163.
(41) Rao, C. V.; Cabrera, C. R.; Ishikawa, Y. Graphene-Supported PtAu Alloy Nanoparticles: A Highly Efficient Anode for Direct Formic Acid Fuel Cells. *J. Phys. Chem. C* **2011**, *115*, 21963−21970.
(42) Zhang, S.; Shao, Y.; Liao, H.-g.; Liu, J.; Aksay, I. A.; Yin, G.; Lin, Y. Graphene Decorated with PtAu Alloy Nanoparticles: Facile Synthesis and Promising Application for Formic Acid Oxidation. *Chem. Mater.* **2011**, *23*, 1079−1081.
(43) Mukherjee, B.; Smith, Y. R.; Subramanian, V. CdSe Nanocrystal Assemblies on Anodized TiO_2 Nanotubes: Optical, Surface, and Photoelectrochemical Properties. *J. Phys. Chem. C* **2012**, *116*, 15175−15184.
(44) Jayashree, R. S.; Spendelow, J. S.; Yeom, J.; Rastogi, C.; Shannon, M. A.; Kenis, P. J. A. Characterization and Application of Electrodeposited Pt, Pt/Pd, and Pd Catalyst Structures for Direct Formic Acid Micro Fuel Cells. *Electrochim. Acta* **2005**, *50*, 4674−4682.
(45) Hwang, S.; Lee, M. C.; Choi, W. Highly Enhanced Photocatalytic Oxidation of CO on Titania Deposited with Pt Nanoparticles: Kinetics and Mechanism. *Appl. Catal., B* **2003**, *46*, 49−63.
(46) Vijayaraghavan, G.; Stevenson, K. J. Synergistic Assembly of Dendrimer-Templated Platinum Catalysts on Nitrogen-Doped Carbon Nanotube Electrodes for Oxygen Reduction. *Langmuir* **2007**, *23*, 5279−5282.
(47) Sun, B.; Smirniotis, P. G.; Boolchand, P. Visible Light Photocatalysis with Platinized Rutile TiO_2 for Aqueous Organic Oxidation. *Langmuir* **2005**, *21*, 11397−11403.
(48) Teranishi, T.; Hosoe, M.; Tanaka, T.; Miyake, M. Size Control of Monodispersed Pt Nanoparticles and Their 2D Organization by Electrophoretic Deposition. *J. Phys. Chem. B* **1999**, *103*, 3818−3827.
(49) Teng, X.; Black, D.; Watkins, N. J.; Gao, Y.; Yang, H. Platinum-Maghemite Core−Shell Nanoparticles Using a Sequential Synthesis. *Nano Lett.* **2003**, *3*, 261−264.
(50) Mandal, S.; Roy, D.; Chaudhari, R. V.; Sastry, M. Pt and Pd Nanoparticles Immobilized on Amine-Functionalized Zeolite: Excellent Catalysts for Hydrogenation and Heck Reactions. *Chem. Mater.* **2004**, *16*, 3714−3724.
(51) Mu, Y.; Liang, H.; Hu, J.; Jiang, L.; Wan, L. Controllable Pt Nanoparticle Deposition on Carbon Nanotubes as an Anode Catalyst for Direct Methanol Fuel Cells. *J. Phys. Chem. B* **2005**, 22212−22216.
(52) Jiang, S. P.; Liu, Z.; Tang, H. L.; Pan, M. Synthesis and Characterization of PDDA-Stabilized Pt Nanoparticles for Direct Methanol Fuel Cells. *Electrochim. Acta* **2006**, *51*, 5721−5730.
(53) Yang, S.; Lee, H. Atomically Dispersed Platinum on Gold Nano-Octahedra with High Catalytic Activity on Formic Acid Oxidation. *ACS Catal.* **2013**, *3*, 437−443.
(54) Hayden, B. E.; Malevich, D. V.; Pletcher, D. Platinum Catalysed Nanoporous Titanium Dioxide Electrodes in H_2SO_4 Solutions. *Electrochem. Commun.* **2001**, *3*, 395−399.
(55) Macak, J. M.; Barczuk, P. J.; Tsuchiya, H.; Nowakowska, M. Z.; Ghicov, A.; Chojak, M.; Bauer, S.; Virtanen, S.; Kulesza, P. J.; Schmuki, P. Self-Organized Nanotubular TiO_2 Matrix as Support for Dispersed Pt/Ru Nanoparticles: Enhancement of the Electrocatalytic Oxidation of Methanol. *Electrochem. Commun.* **2005**, *7*, 1417−1422.
(56) Liu, B.; Chen, J. H.; Zhong, X. X.; Cui, K. Z.; Zhou, H. H.; Kuang, Y. F. Preparation and Electrocatalytic Properties of Pt-SiO_2

Nanocatalysts for Ethanol Electrooxidation. *J. Colloid Interface Sci.* **2007**, *307*, 139−144.
(57) Waszczuk, P.; Lu, G. Q.; Wieckowski, A.; Lu, C.; Rice, C.; Masel, R. I. UHV and Electrochemical Studies of CO and Methanol Adsorbed at Platinum/Ruthenium Surfaces, and Reference to Fuel Cell Catalysis. *Electrochim. Acta* **2002**, *47*, 3637−3652.
(58) Rice, C.; Ha, S.; Masel, R. I.; Wieckowski, A. Catalysts for Direct Formic Acid Fuel Cells. *J. Power Sources* **2003**, *115*, 229−235.
(59) Jiang, K.; Cai, W. B. Carbon Supported Pd-Pt-Cu Nanocatalysts for Formic Acidelectrooxidation: Synthetic Screening and Componential Functions. *Appl. Catal., B* **2014**, *140*, 185−192.
(60) Kucernak, A. R.; Offer, G. J. The Role of Adsorbed Hydroxyl Species in the Electrocatalytic Carbon Monoxide Oxidation Reaction on Platinum. *Phys. Chem. Chem. Phys.* **2008**, *10*, 3699−3711.
(61) Feliu, J. M.; Orts, J. M.; Femandez-Vega, A.; Aldaz, A. Electrochemical Studies in Sulfuric Acid Solutions of Adsorbed CO on Pt (111) Electrodes. *J. Electroanal. Chem.* **1990**, *296*, 191−201.
(62) Lu, G. Q.; Crown, A.; Wieckowski, A. Formic Acid Decomposition on Polycrystalline Platinum and Palladized Platinum Electrodes. *J. Phys. Chem. B* **1999**, *103*, 9700−9711.
(63) Waszczuk, P.; Barnard, T. M.; Rice, C.; Masel, R. I.; Wieckowski, A. A Nanoparticle Catalyst with Superior Activity for Electrooxidation of Formic Acid. *Electrochem. Commun.* **2002**, *4*, 599−603.
(64) He, C.; Ya, X.; Zhu, X. H.; Li, X. Z. A Platinised TiO_2 Film with Both Photocatalytic and Non-Photocatalytic Activities towards the Oxidation of Formic Acid. *Appl. Catal., A* **2004**, *275*, 55−60.
(65) Shu, D.; He, C.; Ya, X.; Meng, Y. Z. Preparation, Characterization and Photoelectrochemical Activities of Platinum-Deposited Titanium Dioxide Film Electrode. *Bull. Electrochem.* **2004**, *20*, 283−288.
(66) Kim, D. H.; Anderson, M. A. Solution Factors Affecting the Photocatalytic and Photoelectrocatalytic Degradation of Formic Acid Using Supported TiO_2 Thin Films. *J. Photochem. Photobiol., A* **1996**, *94*, 221−229.
(67) Rice, C.; Ha, R. I.; Masel, R. I.; Waszczuk, P.; Wieckowski, A.; Barnard, T. Direct Formic Acid Fuel Cells. *J. Power Sources* **2002**, *111*, 83−89.
(68) Park, S.; Xie, Y.; Weaver, M. J. Electrocatalytic Pathways on Carbon-Supported Platinum Nanoparticles: Comparison of Particle-Size-Dependent Rates of Methanol, Formic Acid, and Formaldehyde Electrooxidation. *Langmuir* **2002**, *18*, 5792−5798.
(69) Huang, J. S.; Hou, H. Q.; You, T. Y. Highly Efficient Electrocatalytic Oxidation of Formic Acid by Electrospun Carbon Nanofiber-Supported Pt_xAu_{100-x} Bimetallic Electrocatalyst. *Electrochem. Commun.* **2009**, *11*, 1281−1284.
(70) Chen, Y. X.; Heinen, M.; Jusys, Z.; Behm, R. J. Kinetics and Mechanism of the Electrooxidation of Formic Acid-Spectroelectrochemical Studies in a Flow Cell. *Angew. Chem., Int. Ed.* **2006**, *45*, 981−985.
(71) Liu, Z.; Hong, L.; Tham, M. P.; Lim, T. H.; Jiang, H. Nanostructured Pt/C and Pd/C Catalysts for Direct Formic Acid Fuel Cells. *J. Power Sources* **2006**, *161*, 831−835.
(72) Habibi, B.; Delnavaz, N. Electrocatalytic Oxidation of Formic Acid and Formaldehyde on Platinum Nanoparticles Decorated Carbon-Ceramic Substrate. *Int. J. Hydrogen Energy* **2010**, *35*, 8831−8840.
(73) Wang, J.; Holt-Hindle, P.; MacDonald, D.; Thomas, D. F.; Chen, A. Synthesis and Electrochemical Study of Pt-Based Nanoporous Materials. *Electrochim. Acta* **2008**, *53*, 6944−6952.
(74) Tripkovic, A. V.; Popovic, K. D.; Lovic, J. D.; Markovic, N. M.; Radmilovic, V. Formic Acid Oxidation on Pt/Ru Nanoparticles: Temperature Effects. *Curr. Res. Adv. Mater. Processes* **2005**, *494*, 223−228.
(75) Ahn, M.; Kim, J. Insights into the Electrooxidation of Formic Acid on Pt and Pd Shells on Au Core Surfaces via SERS at Dendritic Au Rod Electrodes. *J. Phys. Chem. C* **2013**, *117*, 24438−24445.
(76) Park, S.; Xie, Y.; Weaver, M. J. Electrocatalytic Pathways on Carbon-Supported Platinum Nanoparticles: Comparison of Particle-Size-Dependent Rates of Methanol, Formic Acid, and Formaldehyde Electrooxidation. *Langmuir* **2002**, *18*, 5792−5798.
(77) Kim, Y.; Kim, H. J.; Kim, Y. S.; Choi, S. M.; Seo, M. H.; Kim, W. B. Shape- and Composition-Sensitive Activity of Pt and PtAu Catalysts for Formic Acid Electrooxidation. *J. Phys. Chem. C* **2012**, *116*, 18093−8100.
(78) Chen, J.; Ollis, D. F.; Rulkens, W. H.; Bruning, H. Kinetic Processes of Photocatalytic Mineralization of Alcohols on Metallized Titanium Dioxide. *Water Res.* **1999**, *33*, 1173−1180.
(79) Turchi, C. S.; Ollis, D. F. Photocatalytic Degradation of Organic-Water Contaminants - Mechanisms Involving Hydroxyl Radical Attack. *J. Catal.* **1990**, *122*, 178−192.
(80) Marugan, J.; Hufschmidt, D.; Lopez-Munoz, M. J.; Selzer, V.; Bahnemann, D. Photonic Afficiency for Methanol Photooxidation and Hydroxyl Radical Generation on Silica-Supported TiO_2 Photocatalysts. *Appl. Catal., B* **2006**, *62*, 201−207.
(81) Hufschmidt, D.; Bahnemann, D.; Testa, J. J.; Emilio, C. A.; Litter, M. I. Enhancement of the Photocatalytic Activity of Various TiO_2 Materials by Platinisation. *J. Photochem. Photobiol., A* **2002**, *148*, 223−231.
(82) Carp, O.; Huisman, C. L.; Reller, A. Photoinduced Reactivity of Titanium Dioxide. *Prog. Solid State Chem.* **2004**, *32*, 33−177.
(83) Spendelow, J. S.; Lu, G. Q.; Kenis, P. J.; Wieckowski, A. Electrooxidation of Adsorbed CO on Pt(1 1 1) and Pt(1 1 1)/Ru in Alkaline Media and Comparison with Results from Acidic Media. *J. Electroanal. Chem.* **2004**, *568*, 215−224.
(84) Lu, G. Q.; Waszczuk, P.; Wieckowski, A. Oxidation of CO Adsorbed from CO Saturated Solutions on the Pt(111)/Ru Electrode. *J. Electroanal. Chem.* **2002**, *532*, 49−55.
(85) Bahnemann, D. W.; Hilgendorff, M.; Memming, R. Charge Carrier Dynamics at TiO_2 Particles: Reactivity of Free and Trapped Holes. *J. Phys. Chem. B* **1997**, *101*, 4265−4275.
(86) Subramanian, V.; Wolf, E. E.; Kamat, P. V. Green Emission to Probe Photoinduced Charging Events in ZnO-Au Nanoparticles. Charge Distribution and Fermi-Level Equilibration. *J. Phys. Chem. B* **2003**, *107*, 7479−7485.
(87) Cuesta, A.; Cabello, G.; Osawa, M.; Gutierrez, C. Mechanism of the Electrocatalytic Oxidation of Formic Acid on Metals. *ACS Catal.* **2012**, *2*, 728−738.